2003

Nonlocal bacterial electron transfer to hematite surfaces

Kevin Rosso
Pacific Northwest National Laboratory, kevin.rosso@pnl.gov

John M. Zachara
Pacific Northwest National Laboratory, john.zachara@pnl.gov

James K. Fredrickson
Pacific Northwest National Laboratory, jim.fredrickson@pnl.gov

Yuri Gorby
Pacific Northwest National Laboratory

Steven Smith
Pacific Northwest National Laboratory, steven.smith@pnl.gov

Pergamon

Geochimica et Cosmochimica Acta, Vol. 67, No. 5, pp. 1081–1087, 2003

0016-7037/03 $30.00 + .00

PII S0016-7037(02)00904-3

Nonlocal bacterial electron transfer to hematite surfaces

KEVIN M. ROSSO,* JOHN M. ZACHARA, JIM K. FREDRICKSON, YURI A. GORBY and STEVEN C. SMITH
Pacific Northwest National Laboratory, P.O. Box 999, K8-96, Richland, WA 99352, USA

(*Received September* 25, 2001; *accepted in revised form March* 27, 2002)

Abstract—Mechanisms by which dissimilatory iron-reducing bacteria utilize iron and manganese oxide minerals as terminal electron acceptors for respiration are poorly understood. In the absence of exogenous electron shuttle compounds, extracellular electron transfer is generally thought to occur through the interfacial contact area between mineral surfaces and attached cells. Possible alternative reduction pathways have been proposed based on the discovery of a link between an excreted quinone and dissimilatory reduction. In this study, we utilize a novel experimental approach to demonstrate that *Shewanella putrefaciens* reduces the surface of crystalline iron oxides at spatial locations that are distinct from points of attachment. *Copyright © 2003 Elsevier Science Ltd*

1. INTRODUCTION

Dissimilatory metal reducing bacteria (DMRB) are common in groundwaters and sediments (Coates et al., 1995; Fredrickson and Gorby, 1996), and substantially influence the aqueous geochemistry and mineralogy of these environments under anoxic conditions (Lovley et al., 1990; Baedecker et al., 1993; Chapelle, 1993; Lovley and Chapelle, 1995; Bennett et al., 1996). At circumneutral pH, this group of microorganisms (including *Geobacter*, *Shewanella*, and others) couple the oxidation of organic matter or H_2 with the reduction of insoluble Fe(III) or Mn(III/IV) oxide minerals to gain energy for maintenance and growth when other thermodynamically favored substrates have been depleted.

Despite intense study, the mechanisms of electron transfer to the oxide phase remain poorly understood. Direct contact between the DMRB and the oxide surface appears to be required for reduction to occur (Arnold et al., 1988; Myers and Nealson, 1988; Lovley et al., 1991; Nevin and Lovley, 2000), unless exogenous electron shuttle agents are present (Lovley et al., 1996; Lovley et al., 1998). Although the apparent need for direct contact does not implicate a mechanistic pathway, it in large part has led to the prevailing conceptual model that electron transfer to the oxides, and therefore destabilization of surface metal sites promoting dissolution of the oxide phase, is restricted to the interfacial area at the cell–oxide contact. This model has not been successfully confirmed by microscopic observations, despite efforts to do so (Grantham et al., 1997).

The possibility of alternative reduction pathways for *Shewanella* obviating the requirement for direct cell–oxide contact has recently been proposed based on the discovery of a link between a biosynthesized quinone serving as a suspected extracellular electron shuttle compound, and the dissimilatory reduction of a variety of electron acceptors (Newman and Kolter, 2000). In this study, we utilize a novel experimental approach to demonstrate that *Shewanella* reduces/dissolves the surface of crystalline Fe(III) oxides at spatial locations that are distinct from points of attachment. We performed a series of atomic force microscopy (AFM) experiments to probe well-characterized basal surfaces of hematite single crystals for dissolution features arising from controlled exposure to the DMRB *Shewanella putrefaciens* CN32. The novelty lies in the fact that the size of individual crystallites is much larger than the size of the microorganisms, allowing us to observe the spatial relationships between surface structure, cell locations, and sites of preferred dissolution. Our results indicate that this DMRB applies a nonlocal electron transfer pathway to reduce crystalline Fe(III) oxides under the specific conditions of this study.

2. METHODS

Euhedral tabular single crystal platelets of pure hematite were produced using a hydrothermal technique (Sapieszko and Matijevic, 1980). Platelet sizes were typically 20 μm across and 1 to 2 μm thick. CN32 was isolated from a sedimentary aquifer and can reduce noncrystalline and crystalline Fe(III) oxides (Fredrickson et al., 1998; Zachara et al., 1998). Hematite samples were incubated with CN32 under anoxic conditions in bicarbonate buffered medium (pH = 6.8) using lactate as the electron donor, as described below. During the course of this work, based on Fe(II) analyses of the aqueous phase, it was found that bioreduction was initially fast and tapered off to very slow reduction rates. Reinoculation was used to advance the development of bioreduction features on the hematite surfaces, with subsamples collected between inoculations, as detailed below.

Hematite suspensions were prepared in an anoxic chamber using the following steps. Hematite powder (80 mg) was placed in 20-mL glass headspace vials where 5 mL of anoxic 0.1 mol/L $NaClO_4$ and 4 mL of filter sterilized anoxic bacterial growth media at 2.5× concentration were added to each vial. The final concentrations of media components were 1.34 mM KCl, 28.0 mM NH_4Cl, 0.68 mM $CaCl_2$, 20.0 mM lactate, 0.4 mM H_3PO_4, and 30.0 mM HCO_3^-. The pH was adjusted to 6.8 using anoxic 6 mol/L NaOH. The headspace atmosphere was then purged with an N_2:CO_2 (80:20) gas mixture for 5 min. *S. putrefaciens* strain CN32 (1 mL) was added to select tubes, and 1 mL of anoxic water was added to remaining tubes designated as abiotic controls. The above sets were duplicated for the case

* Author to whom correspondence should be addressed (kevin.rosso@pnl.gov).

of including anthraquinone-2,6-disulfonate (AQDS), in which case anoxic AQDS was added until a final concentration of 0.1 mM AQDS was reached before the CN32 addition step. The suspensions were then incubated anoxically in a shaker bath at 30°C in the dark.

Subsamples were collected over 6- to 10-d intervals, at which time the sampled vials were discarded, and remaining vials were prepared for reinoculation, described below. The sampling included the Fe(II) and total Fe in the aqueous phase, the HCl extractable Fe(II) and total Fe, and hematite solids. The aqueous phase in each vial was sampled by transferring 2 mL of the suspension to a plastic syringe fitted with a 0.2-μm filter. The first 20 drops of filtrate were discarded and the next 9 were collected in a 5-mL polystyrene tube with 0.5 mL of 1 mol/L anoxic HCl for Fe analysis. The HCl extractable Fe in each vial was sampled by transferring 0.2 mL of the suspension to a 4-mL polystyrene tube containing 3.8 mL anoxic 0.53 mol/L HCl. The tubes were removed from the anoxic chamber and placed in an incubator-shaker at 30°C at 100 rpm for 20 h. The tubes were returned to the anoxic chamber and 0.2 mm of the suspension was transferred to a plastic syringe fitted with a 0.2-μm filter. The first 20 drops of filtrate were discarded and the remaining collected in a polystyrene tube for Fe analysis.

Hematite solids in each vial were sampled by transferring 400 mL of the suspension to a 5-mL polystyrene tube with 3.6 mL of anoxic 0.53 mol/L HCl. The tubes were place in an incubator-shaker at 30°C for 20 h. The suspension was transferred to a plastic syringe fitted with a 2-μm filter. All liquid was pushed through the filter, leaving the hematite residue on the filter. The hematite residue on the filter was rinsed three times with anoxic water, then three times with anoxic 0.1 mol/L $NaHCO_3$, then three times with anoxic water, and then air dried. The procedure described above results in hematite surfaces which are free of any reduced Fe and therefore stable in air. These solids were used for surface microtopographic analysis by AFM in air as described below.

Vials that were not sampled were prepared for reinoculation in the following manner. Suspensions were transferred to polycarbonate tubes and centrifuged at 10,000 relative centrifugal force (rcf) for 1 h, after which the supernatant was discarded. 20 mL of anoxic 0.1 mol/L $NaClO_4$ was added and the solids resuspended, recentrifuged, and supernatant discarded again. 30 mL of anoxic 0.5 mol/L HCl was added and the suspensions were placed in an incubator-shaker at 30°C for 20 h to remove extractable Fe. The suspensions were then centrifuged at 10,000 rcf for 1 h and the supernatant discarded. Three similar washes were then performed using 20 mL of anoxic 0.1 mol/L $NaClO_4$. The solids were then resuspended in anoxic 0.1 mol/L $NaClO_4$ and 5-mL portions were added to glass headspace vials for the addition of media and reinoculation with CN32 following the steps as previously described. Using these procedures, sets of four incrementally bioreduced samples of hematite platelets and corresponding aqueous Fe analyses were produced for cases where AQDS was and was not included in the experiments.

AFM was performed in air under ambient conditions using a Digital Instruments, Inc. BioScope operating in contact mode. A fraction of the air-dried hematite solids were mounted on glass microscope slides using the thermoplastic adhesive Tempfix. Standard Si_3N_4 probes were used, having a nominal radius of curvature of 20 to 60 nm and an approximate spring constant of 0.12 N/m for the chosen cantilever. Imaging washed, air-dried samples in air provided the important advantage over imaging in water that no loosely bound material was present on the surface. In air, cellular material is strongly bound to the hematite surface and was found to be immovable by the AFM tip. AFM tips did not collect material, and consequently imaging quality remained consistently high over many hours of scanning. No disturbances of material on the hematite surfaces by the tip could be intentionally produced by manipulation of the applied forces, nor were observed during data collection at any time. Contact forces were minimized for data collection. Scan rates varied from 0.5 to 1.0 Hz. The differences in the quantities displayed between topographic and deflection image data are inconsequential for the purposes of this study. The grayscale of topographic image data scales linearly with the actual height of features being measured. Deflection data often better reveal the presence of topographic features. Therefore, because of image contrast issues, the desired information can sometime be better conveyed by one or the other. Both are presented where deemed useful.

3. RESULTS AND DISCUSSION

Using AFM, we first characterized the surface microtopography of the unreduced hematite platelets so that microbial dissolution features could later be identified. Detailed studies of the surfaces of natural hematites have established that that basal plane is formed by two-dimensional spreading of growth layers from imperfections in the crystal structure (Sunagawa, 1960; Sunagawa, 1962). The imperfections result from the build-up of internal stress as growth proceeds and are concentrated near the growth centers. Structural features on the hematite surfaces used in this study were consistent with this growth mechanism. The basal surfaces invariably displayed large atomically flat terraces that continued for several microns before termination at a step (Fig. 1). Growth layers typically consisted of groupings of monomolecular hematite layers, forming small steps (1 to 15 nm high) across the surface. Steps were concentrically arranged around growth centers located in the interior portions of the platelets. Growth centers were well-defined and limited in number on each platelet, consistent with preferential nucleation at structural defects. We therefore concluded that structurally strained regions were present near the growth centers in the majority of the hematite crystallites used in this study.

After the exposures to DMRB, evidence for microbial reductive dissolution was demonstrated in both the aqueous Fe analyses and AFM images of microbially reduced oxide. Total aqueous Fe was predominantly in the +2 oxidation state, indicating that the bacteria were utilizing ferric iron in the hematite as the terminal electron acceptor (Fig. 2). Dilute HCl treatment of the solids extracted sorbed, biogenic Fe(II) of unknown physiochemical state that was present in nearly equimolar concentration to aqueous Fe(II) (data not shown). The concentration of biogenic Fe(II) decreased with each successive inoculation cycle, suggesting that the reducible Fe(III) at the hematite surface, while never exhausted, was of increasingly lower bioavailability to the bacteria with time. The presence of AQDS increased the amount of biogenic Fe(II) as expected (Fig. 2), consistent with the prevalent view that it

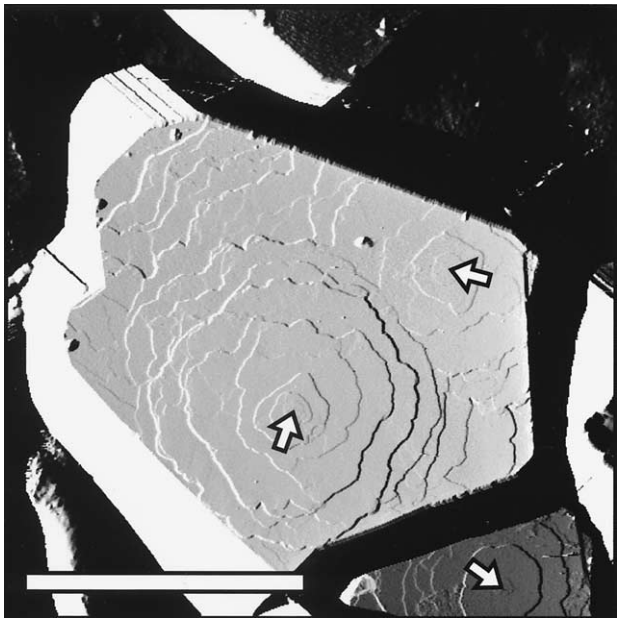

Fig. 1. AFM image (deflection) showing layer growth features on the basal surface typical of the tabular hematites used in this study (Scale bar = 10 μm). Step heights are nominally 1 to 15 nm. Growth centers (marked by arrows) were few and well defined on each crystallite by the concentrically arranged steps. Concentrations of bulk defects are located at the apices of these features.

mediates electron transfer between metal reducing bacteria and mineral surfaces (Lovley et al., 1996; Zachara et al., 1998).

Based on the current cell–oxide contact model, it was expected that dissolution features across DMRB-reduced oxide surfaces would be located at points where respiring bacteria had been attached. Using AFM, the dissolution features that were found markedly contrasted with this expectation. The

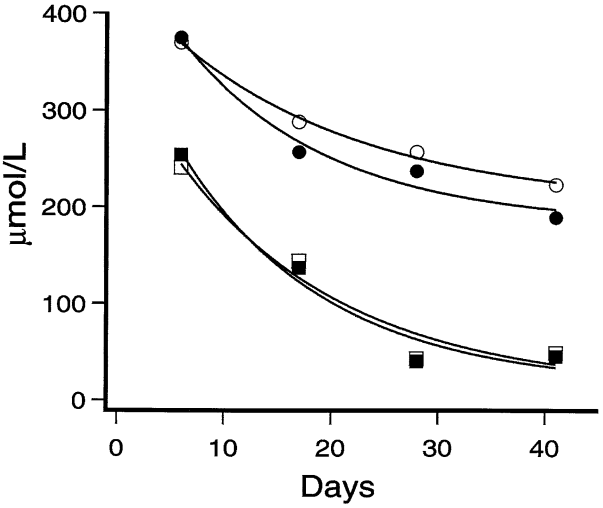

Fig. 2. Total [Fe(III) + Fe(II)] iron (open markers) and [Fe(II)] (filled markers) measured concentrations in the aqueous phase after four successive inoculations with (circles) and without (squares) the presence of AQDS. For all abiotic control samples, total Fe in aqueous phase was below detection limits (<3 μmol/L).

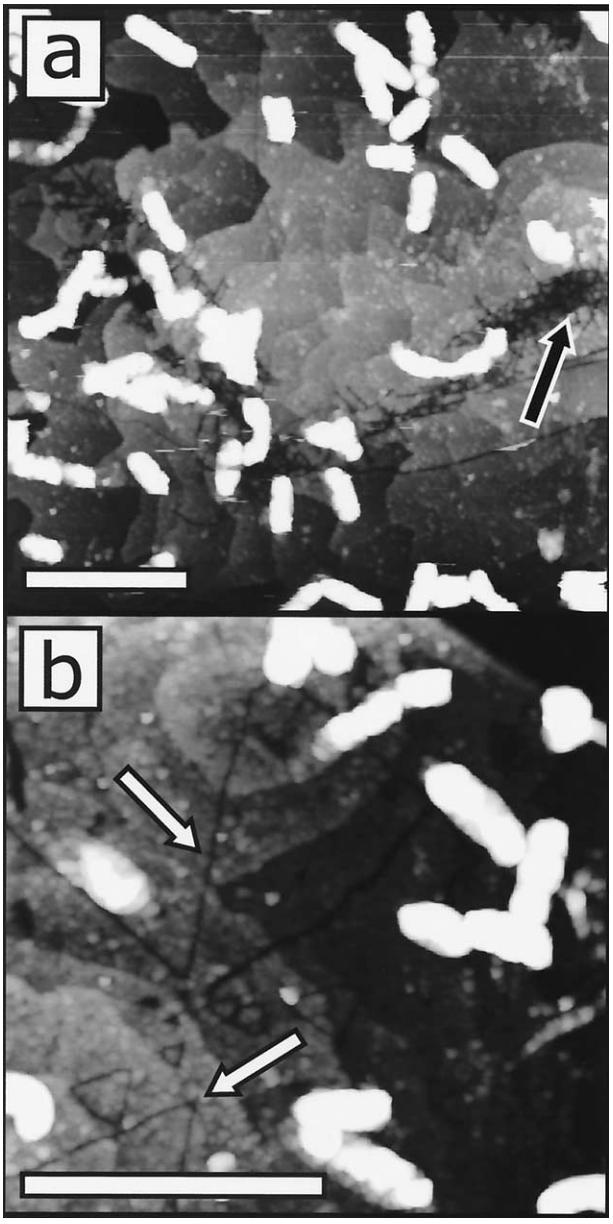

Fig. 3. AFM images (topographic) of hematite grains bioreduced by *Shewanella*. (Scale bars = 4 μm). Cell distributions were not found to correlate with surface microtopography. Reductive dissolution features routinely found were (a) micron-scale etching localized at the apices of growth centers as indicated by the black arrow and (b) structurally controlled etch channels, some examples of which are indicated by white arrows, often radiating outward along what are likely dislocation networks in the bulk structure.

dissolution features can be characterized by two distinct types: 1) prominent bulk defect controlled micron-scale etch pits (Figs. 3 and 4), and 2) uniformly distributed shallow etch pits <500 nm in size (Fig. 5). The former were localized at the apices of growth centers (Fig. 3a and Fig. 4) and often radiated outward along structurally controlled directions (see Fig. 3b and Fig. 4); the latter were randomly distributed across atomically flat terraces and were occasionally triangular in shape (e.g., Fig. 3b), consistent with the hexagonal hematite structure.

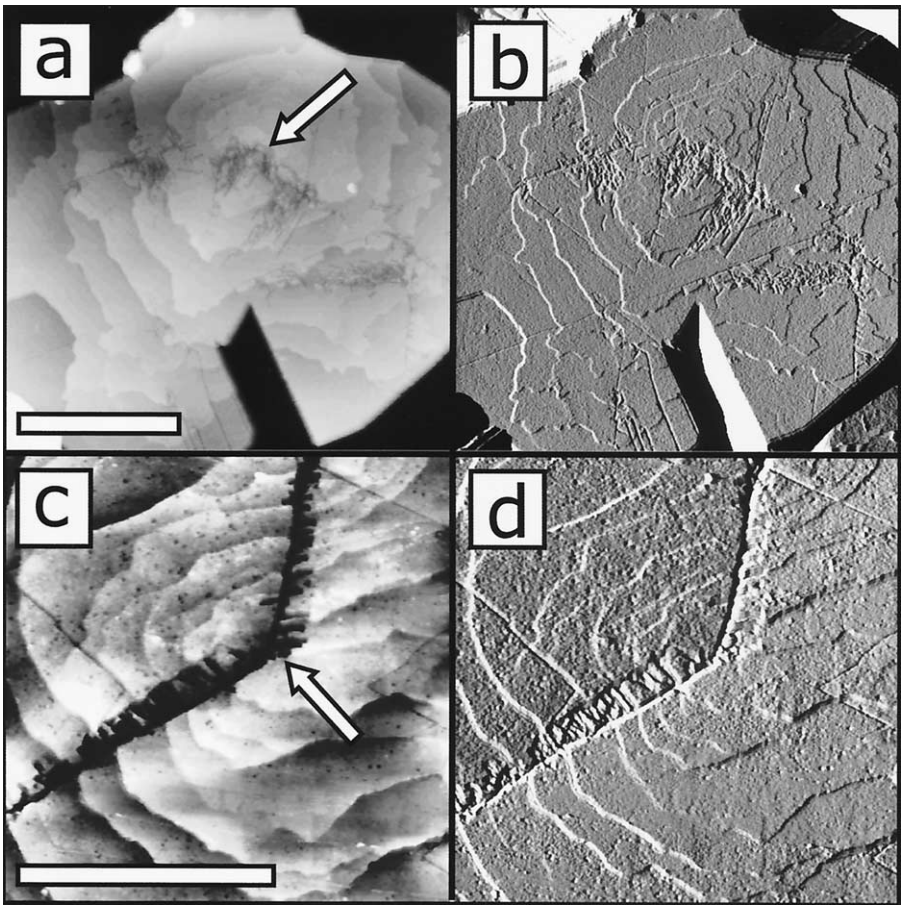

Fig. 4. Topographic (a,c) and deflection (b,d) AFM images showing reductive dissolution features on hematite crystallites displaying no independent evidence of prior cell attachment (Scale bar = 4 μm). The upper set of images show that dissolution was most facile at the apex of the prominent growth center, indicated by an arrow, and along structurally controlled linear channels across the surface. The lower set of images show advanced dissolution along what is likely a misfit boundary between two slightly misoriented crystallites, along with random nanometer-scale etching of flat terraces. The main dissolution feature is the dark jagged trench running from the left side of the image to the center and there bending upwards to the image top. The location of the apex of the growth center is indicated by an arrow.

Neither of these features were associated with the starting material (i.e., Fig. 1). The features were not found on any of the abiotic controls run in parallel (Fig. 6). The surface features only arose when the DMRB was present in the experiments. The etch features were consistently observed on all bioreduced hematite platelets independent of the presence of AQDS.

Because our procedure did not remove attached cells, samplings effectively captured snapshots of surface-associated cells as well as residual organic cellular debris that remained on the cell surface as a "footprint" after a cell had detached. Attached cells were routinely found on most platelets and cell size, shape, or distribution across the surface was unrelated to the dissolution structures. Densely populated crystallites did not show enhanced dissolution features relative to sparsely populated crystallites. Dissolution features were present at crystallite locations where there was no independent evidence of prior cell attachment (see Fig. 4). Locations of cell attachment with subsequent detachment were found on some crystallites where rimmed, aggregate features were observed demarking a cell "footprint" on the basal surface (Fig. 7). These "bleb-like" features have been attributed to residual outer membrane vesicles (Gorby et al., 2002). The random distribution of the nanometer-scale etch pits clearly cannot be attributed to prior uniform cell coverage because detached cell locations were demarked by these features. Although we cannot rule out that reductive dissolution was also occurring at cell–oxide contacts, no evidence of enhanced dissolution could be found using high-resolution AFM imaging of regions around the periphery of these features. These results suggest that dissolution was not localized in the vicinity of cell–oxide interfaces.

In contrast to the current cell–oxide contact model, these features are clearly in accord with surface controlled chemical dissolution behavior, where dissolution is controlled by solute interactions with reactive surface sites, as opposed to being controlled by direct electron transfer through cell–oxide contacts at populated regions of the surface. A chemical dissolution mechanism would principally attack the energetically unstable surface sites at the areas of localized structural strain, such as the surface penetration points for structural defects near the growth centers. This mechanism is consistent with the evolution trend of biogenic Fe(II) (Fig. 2), where decreasing bioavailability with increasing inoculation number may result

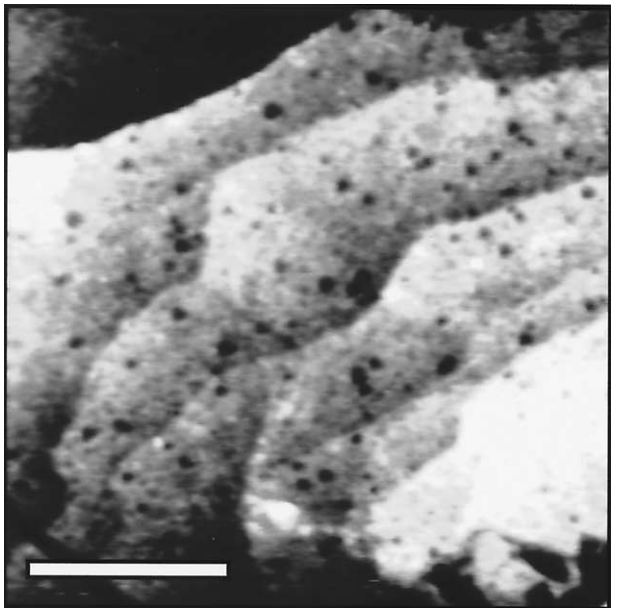

Fig. 5. AFM image (topographic) showing shallow nanometer-scale etching (dark spots) of otherwise atomically flat terraces on the basal plane of a hematite crystallite (Scale bar = 1 μm). Etch pit distributions are random and cannot be related to cell size, shape, or distribution. This form of etch is consistent with dissolution at point defects across the surface.

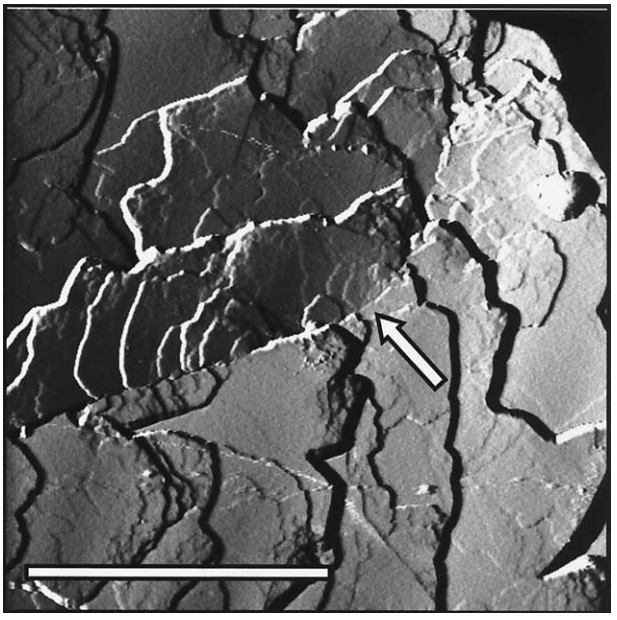

Fig. 6. AFM image (deflection) showing the surface of one of the control hematite samples (Scale bar = 4 μm). No dissolution features were found on the control surfaces. This image shows what is likely a misfit boundary in the crystallite, a structurally strained area having an increased tendency for dissolution. The misfit boundary runs from the left side of the image toward the center and then inflects up toward the top center. An arrow marks the inflection point. Dissolution features consistent with those observed on the DMRB reacted samples are not found.

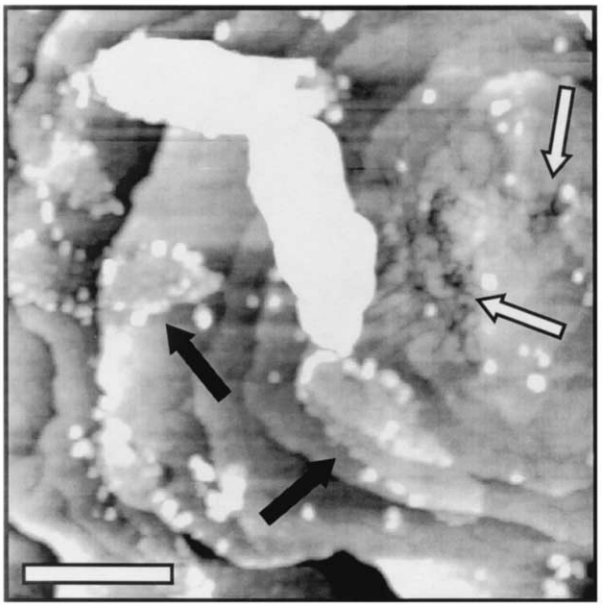

Fig. 7. AFM image (topographic) showing dissolution at the apex of a growth center (white arrows) and cell "footprint" features where detached DMRB cells have left residual matter on the surface (black arrows) (Scale bar = 1 μm). The footprint features have approximately the same lateral dimensions as cells.

from the preferential dissolution and consumption of these defective regions in the crystallites.

We dismiss the possibility that electron transduction from attached cells to reactive defect sites through the hematite lattice could occur with the efficiency necessary to produce the observed dissolution behavior. Based on the microscopic observations of the spatial relationships between attached cells and dissolution features, this would require electric conduction through the hematite near-surface or bulk over micron length scales. Compositionally pure hematite, as was used here, is a poor electrical conductor with a bandgap in the vicinity of 2 *e*V (Mochizuki, 1977; Ma et al., 1993).

For the tabular hematite morphology, preferential chemical etching at structurally defective locations on the basal plane and a "center-outward" progression of dissolution has already been demonstrated previously (Schwertmann and Cornell, 1991; Cornell and Giovanoli, 1993). Likewise, dislocation networks forming misfit boundaries have been shown to possess hexagonal symmetry parallel to the c-axis in hematite (Tietz and Carter, 1993), providing the only reasonable explanation for the striking, structurally controlled, linear dissolution channels radiating outward from the growth centers (e.g., Fig. 4b). The smaller scale random etch pits are consistent with point defect attack. The AFM observations clearly suggest that the microorganisms do not discriminate these types of surface defect sites during attachment and subsequent dissimilatory Fe(III) reduction. Rather, the images suggest that during anaerobic respiration the bacteria release a soluble agent or agents into the medium that causes facile dissolution of these unstable surface sites.

The presence of such an agent is completely inferred. We made no attempts to independently verify that an electron

transfer agent was being biosynthesized by CN32. This task would likely be very challenging and we have therefore reserved it for future work. However, based on recent studies in this area, speculation regarding the nature of this species is possible. For example, it is possible that the soluble species is a "siderophore-like" complexant that solubilizes Fe(III) from the oxide surface rendering it more bioavailable for reduction, or a "quinone-like" reductant that enables electron shuttling between the electron transport system of the DMRB and the oxide surface. *Shewanella* produces siderophores under Fe-limiting conditions (Gram, 1994) capable of promoting Fe(III)-oxide dissolution (Hersman et al., 1995). However, the presence of Fe(II) typically represses siderophore biosynthesis in many gram-negative bacteria (Escolar et al., 1999). Our experimental conditions were not Fe-limiting and therefore it seems unlikely that siderophore production would have been expressed by *Shewanella*. Based on the work of Newman and Kolter (2000), we suspect that the soluble agent is a quinone-like reductant.

We do not suggest that cell attachment is not required for bioreduction to occur. Recent studies on the role of cell attachment continue to point to its importance for DMRB (Nevin and Lovley, 2000). We also cannot completely rule out direct electron transfer. Our data only address the fact that for cells that are not restricted from contacting the hematite surface, an indirect mode of electron transfer is preferred, at least for the specific hematite form and experimental conditions used here. It is fully possible that attachment must first precede, and in some way activate the utilization of such a pathway.

It is noteworthy that the dissolution behavior we observed is in agreement with the microscopic observations of microbial reductive dissolution of Fe(III)-oxide under anaerobic conditions by Grantham et al. (1997). Microcrystalline Fe(III) oxyhydroxide coatings were observed to undergo widespread (nonlocal) dissolution by *Shewanella* under anaerobic conditions, which contrasted with localized, cell-shaped pitting at the cell–oxide contact under aerobic conditions. The coatings were too fine-grained to resolve the dissolution features associated with individual crystallites. No enhanced pitting was observed at the cell–oxide contacts, exposed by controlled mechanical action of the AFM tip. The widespread dissolution behavior under anaerobic conditions was attributed to repeated cell–oxide contact resulting from passive cell mobility across the oxide coating, shorter-lived than image acquisition times. However, it has recently been shown that the strength of attraction of *Shewanella* on goethite (α-FeOOH) is initially 2 to 4 times stronger under anaerobic conditions than aerobic, and that the force required for cell removal increases with attachment duration, indicating that cell mobility is less favorable under anaerobic conditions (Lower et al., 2001). These results suggest that the mobility of attached *Shewanella* on Fe(III) oxide surfaces may be small. When weighed in the context of our microscopic results, there is compelling evidence to suggest that previous conclusions regarding the anaerobic reductive dissolution behavior should be revised. Our model implicates one or more soluble extracellular factors as the electron transducing agents in dissimilatory Fe(III) reduction by *Shewanella*. These soluble agents create localized areas of dissolution surrounding defects that are spatially separated from points of microbial attachment. Whether this strategy is unique to *Shewanella*, or unique to the hematite system specifically, where the energy gain from reduction is small (Zachara et al., 1998; Liu et al., 2001) remains unresolved.

4. CONCLUSIONS

In conclusion, the findings indicate that Fe(III) oxide-reducing *Shewanella* can implement a nonlocal electron transfer strategy. The evidence for significant dissolution beyond the organism footprint suggests that DMR strains of *Shewanella* can mount a generalized attack of oxide minerals that, in effect, allows access to the most soluble or bioavailable regions of the Fe(III) oxide surface. The soluble factor allows electron disposal to energetically favorable surface locations that are spatially removed from the locations of cell attachment. This nonlocal pathway reveals a new and important link between mineral structure and bioreactivity for DMRB/oxide systems. These findings may, in part, explain the relative effectiveness of *Shewanella* in reducing crystalline Fe(III) oxides (Roden and Zachara, 1996; Urrutia et al., 1998; Zachara et al., 1998) as compared to *Geobacter* which apparently does not biosynthesize electron shuttling compounds (Nevin and Lovley, 2000). Our findings do not allow comment on whether direct attachment of *Shewanella* is required for Fe(III) oxide reduction; perhaps biosynthesis of the soluble factor is triggered by the attachment process itself. Regardless, these results suggest that the conceptual model describing dissimilatory reduction of oxide minerals as being restricted to cell–oxide contacts should be modified to include nonlocal electron transfer pathways.

Acknowledgments—Sponsored by the U.S. Department of Energy, Office of Basic Energy Sciences, Engineering and Geosciences Division.

Associate editor: J. P. Amend

REFERENCES

Arnold R. G., DeChristina T. J., and Hoffman M. R. (1988) Reductive dissolution of Fe(III) oxides by *Pseudomonas* sp. 200. *Biotechnol. Bioengin.* **32,** 1081–1096.

Baedecker M. J., Cozzarelli I. M., Siegal D. I., Bennett P. C., and Eganhouse R. P. (1993) Crude oil in shallow sand and gravel aquifer: 3. Biogeochemical reactions and mass balance modeling anoxic groundwater. *Appl. Geochem.* **8,** 569–589.

Bennett P. C., Hiebert F. K., and Choi W. J. (1996) Microbial colonization and weathering of silicates in a petroleum-contaminated groundwater. *Chem. Geol.* **132,** 45–53.

Chapelle F. H. (1993) *Ground-water Microbiology and Geochemistry*. John Wiley & Sons.

Coates J. D., Lonergan D. J., Philips J. P., Jenter H., and Lovley D. R (1995) *Desulfuromonas palmitatis* sp. nov., a marine dissimilatory Fe(III) reducer that can oxidize long-chain fatty acids. *Arch. Microbiol.* **164,** 406–413.

Cornell R. M. and Giovanoli R. (1993) Acid dissolution of hematites of different morphologies. *Clay Minerals* **28,** 223–232.

Escolar L., Perez-Martin J., and De Lorenzo V. (1999) Opening the iron box: Transcriptional metalloregulation by the fur protein. *J. Bacteriol.* **181,** (20) 6223–6229.

Fredrickson J. K. and Gorby Y. A. (1996) Environmental processes mediated by iron-reducing bacteria. *Curr. Opinion Biotechnol.* **7,** 287–294.

Fredrickson J. K., Zachara J. M., Kennedy D. W., Dong H. L., Onstott T. C., Hinman N. W., and Li S. M. (1998) Biogenic iron mineralization accompanying the dissimilatory reduction of hydrous ferric oxide by a groundwater bacterium. *Geochim. Cosmochim. Acta* **62,** (19–20) 3239–3257.

Gorby Y., McLean J., Dohnalkova A., Korenevsky A., Rosso K. M., Beveridge T. J. (2002). Membrane vesicles from the dissimilatory iron-reducing bacterium *Shewanella putrefaciens* strain CN32. *Appl. Environ. Microbiol.* (in press.)

Gram L. (1994) Siderophore-mediated iron sequestering by Shewanella putrefaciens. *Appl. Environ. Microbiol.* **60,** (6) 2132–2136.

Grantham M. C., Dove P. M., and DiChristina T. J. (1997) Microbially catalyzed dissolution of iron and aluminum oxyhydroxide mineral surface coatings. *Geochim. Cosmochim. Acta* **61,** (21) 4467–4477.

Hersman L., Lloyd T., and Sposito G. (1995) Siderophore-promoted dissolution of hematite. *Geochim. Cosmochim. Acta* **59,** (16) 3327–3330.

Liu C. X., Kota S., Zachara J. M., Fredrickson J. K., and Brinkman C. K. (2001) Kinetic analysis of the bacterial reduction of goethite. *Environ. Sci. Technol.* **35,** (12) 2482–2490.

Lovley D. R. and Chapelle F. H. (1995) Deep subsurface microbial processes. *Rev. Geophys.* **33,** (3) 365–381.

Lovley D. R., Chapelle F. H., and Phillips E. J. P. (1990) Fe(III)-reducing bacteria in deeply buried sediments of the Atlantic Coastal Plain. *Geology* **18,** 954–957.

Lovley D. R., Coates J. D., Blunt-Harris E. L., Phillips E. J. P., and Woodward J. C. (1996) Humic substances as electron acceptors for microbial respiration. *Nature* **382,** 445–448.

Lovley D. R., Fraga J. L., Blunt-Harris E. L., Hayes L. A., Phillips E. J. P., and Coates J. D. (1998) Humic substances as a mediator for microbially catalyzed metal reduction. *Acta Hydrochim. Hydrobiol.* **26,** (3) 152–157.

Lovley D. R., Phillips E. J. P., and Lonergan D. J. (1991) Enzymatic versus nonenzymatic mechanisms for Fe(III) reduction in aquatic sediments. *Environ. Sci. Technol.* **25,** (6) 1062–1067.

Lower S. K., Beveridge T. J., and Hochella Jr. M. F. (2001) Electron transfer at the *Shewanella*–iron oxide interface: Fundamental observations of a complex phenomenon. *Science* **292,** 1360–1363.

Ma Y., Johnson P. D., Wassdahl N., Guo J., Skytt P., Nordgren J., Kevan S. D., Rubensson J. -E., Boske T., and Eberhardt W. (1993) Electronic structures of α-Fe_2O_3 and Fe_3O_4 from O K-edge absorption and emission spectroscopy. *Phys. Rev. B* **48,** (4) 2109–2111.

Mochizuki S. (1977) Electrical conductivity of α-Fe_2O_3. *Physica Status Solidi A* **41,** (2) 591–594.

Myers C. R. and Nealson K. H. (1988) Bacterial manganese reduction and growth with manganese oxide as the sole electron acceptor. *Science* **240,** 1319–1321.

Nevin K. P. and Lovley D. R. (2000) Lack of production of electron-shuttling compounds or solubilization of Fe(III) during reduction of insoluble Fe(III) oxide by Geobacter metallireducens. *Appl. Environ. Microbiol.* **66,** (5) 2248–2251.

Newman D. K. and Kolter R. (2000) A role for excreted quinones in extracellular electron transfer. *Nature* **405,** (6782) 94–97.

Roden E. E. and Zachara J. M. (1996) Microbial reduction of crystalline iron(III) oxides: Influence of oxide surface area and potential for cell growth. *Environ. Sci. Technol.* **30,** (5) 1618–1628.

Sapieszko R. S. and Matijevic E. (1980) Preparation of well-defined colloidal particles by thermal decomposition of metal chelates. *J. Colloid Interface Sci.* **74,** (2) 405–422.

Schwertmann U. and Cornell R. M. (1991) *Iron Oxides in the Laboratory Preparation and Characterization.* VCH Publishers.

Sunagawa I. (1960) Growth history of hematite. *Amer. Mineralogist* **45,** 566–575.

Sunagawa I. (1962) Mechanism of growth of hematite. *Amer. Mineralogist* **47,** 1139–1155.

Tietz L. A. and Carter C. B. (1993) Structure of the Fe_2O_3-Al_2O_3 (0001) interface. *Philosophical Magazine A—Physics of Condensed Matter Structure Defects and Mechanical Properties* **67,** (3) 699–727.

Urrutia M. M., Roden E. E., Fredrickson J. K., and Zachara J. M. (1998) Microbial and surface chemistry controls on reduction of synthetic Fe(III) oxide minerals by the dissimilatory iron-reducing bacterium *Shewanella alga*. *Geomicrobiol. J.* **15,** (4) 269–291.

Zachara J. M., Fredrickson J. K., Li S. M., Kennedy D. W., Smith S. C., and Gassman P. L. (1998) Bacterial reduction of crystalline Fe^{3+} oxides in single phase suspensions and subsurface materials. *Amer. Mineralogist* **83,** 1426–1443 (11–12).